

The reliability of [CII] as a star formation rate indicator

Ilse De Looze¹, Maarten Baes¹, George J. Bendo², Luca Cortese³ and Jacopo Fritz¹

¹*Sterrenkundig Observatorium, Universiteit Gent, Krijgslaan 281 S9, B-9000 Gent, Belgium*

²*UK ALMA Regional Centre Node, Jodrell Bank Centre for Astrophysics, School of Physics and Astronomy, University of Manchester, Oxford Road, Manchester M13 9PL, United Kingdom*

³*European Southern Observatory, Karl-Schwarzschild Str. 2, 85748 Garching bei Muenchen, Germany*

Received 25 December 2010

ABSTRACT

The [CII] 157.74 μm line is an important coolant for the neutral interstellar gas. Since [CII] is the brightest spectral line for most galaxies, it is a potentially powerful tracer of star formation activity. In this paper we present a calibration of the star formation rate as a function of the [CII] luminosity for a sample of 24 star-forming galaxies in the nearby universe. This sample includes objects classified as HII regions or LINERs, but omits all Seyfert galaxies with a significant AGN contribution to the mid-infrared photometry. In order to calibrate the SFR against the line luminosity, we rely on both GALEX FUV data, which is an ideal tracer of the unobscured star formation, and MIPS 24 μm , to probe the dust-enshrouded fraction of star formation. In case of normal star-forming galaxies, the [CII] luminosity correlates well with the star formation rate. However, the extension of this relation to more quiescent ($H\alpha$ EW ≤ 10 Å) or ultraluminous galaxies should be handled with caution, since these objects show a non-linearity in the $L_{[\text{CII}]}$ -to- L_{FIR} ratio as a function of L_{FIR} (and thus, their star formation activity).

We provide two possible explanations for the origin of the tight correlation between the [CII] emission and the star formation activity on a global galaxy-scale. A first interpretation could be that the [CII] emission from PDRs arises from the immediate surroundings of star-forming regions. Since PDRs are neutral regions of warm dense gas at the boundaries between HII regions and molecular clouds and they provide the bulk of [CII] emission in most galaxies, we believe that a more or less constant contribution from these outer layers of photon-dominated molecular clumps to the [CII] emission provides a straightforward explanation for this close link between the [CII] luminosity and SFR. Alternatively, we consider the possibility that the [CII] emission is associated to the cold ISM, which advocates an indirect link with the star formation activity in a galaxy through the Schmidt law.

Key words: galaxies: star formation – ISM: lines and bands – infrared: galaxies – ultraviolet: galaxies

1 INTRODUCTION

The [CII] line is an important coolant of the neutral interstellar medium (ISM), heated through the photoelectric effect on dust grains and Polycyclic Aromatic Hydrocarbons (PAHs), that have been exposed to ultraviolet (UV) photons. This UV emission can originate both in HII regions, the diffuse neutral and ionized interstellar medium (Nakagawa et al. 1998; Wolfire 1995) and in PhotoDissociation Regions (PDRs) (Crawford et al. 1985; Tielens & Hollenbach 1985; Wolfire et al. 1989; Hollenbach et al. 1991; Stacey et al. 1991; Bakes & Tielens 1998). Since the [CII] line is generally a very strong line in all star-forming galaxies and in particular for low-metallicity objects (Madden 2000), it is a potentially powerful star formation rate (SFR) indicator. In this paper we aim to quantify the reliability of [CII] as a star formation rate indicator from a sample of galaxies in the nearby universe.

Despite the strength of the [CII] line emission, several issues might obstruct a direct link with the star-forming activity in galaxies. For instance, the ambiguity concerning the origin of the dominant heating source for the interstellar gas, contaminates the correlation between the [CII] line emission and the SFR. Furthermore, this correlation is also affected by the saturation of the [CII] excitation at high temperatures and high densities (Kaufman et al. 1999). Nevertheless, using [CII] as a star formation indicator does benefit from the fact that it is unaffected by extinction in most cases. Exceptions might be extreme starbursts (Luhman et al. 1998; Helou 2000) or edge-on galaxies (Heiles 1994). Recently, Papadopoulos et al. (2010) claimed that the deficiency of [CII] in Arp 220 is due to a high FIR/submm dust optical depth effect and is not caused by saturation of the [CII] excitation in higher density PDRs. Rangwala et al. (2010) (private communication) also confirms that [CII] might be affected by higher optical depths in Arp 220, but they found

much lower values than Papadopoulos et al. (2010). A thorough analysis of this dust obscuration effect at FIR/submm wavelengths in other galaxies with a [CII] deficiency is necessary to give insight on this debated issue.

The Herschel satellite (Pilbratt et al. 2010) is currently making [CII] observations, with the aim of studying the ISM of nearby galaxies. The advent of ALMA will make this line observable at high redshifts (for redshift $z > 2$, the [CII] 157.74 μm line shifts to atmospheric windows at submm/mm wavelengths, which are observable from ground-based facilities). Stark (1997) and Nagamine et al. (2006) already probed the detectability of [CII] in high-redshift galaxies. According to Nagamine et al. (2006) very bright Lyman break galaxies and distant red galaxies are likely candidates to have the most prominent [CII] emission at high redshift. Some detections of [CII] in high-redshift objects already have been reported (Maiolino et al. 2005; Iono et al. 2006; Maiolino et al. 2009; Hailey-Dunsheath et al. 2010; Ivison et al. 2010; Wagg et al. 2010; Stacey et al. 2010).

The [CII] line has been used previously to probe the physical processes in PDRs, but also to detect star formation in nearby galaxies (Genzel & Cesarsky 2000; Malhotra et al. 2001; Boselli et al. 2002; Luhman et al. 2003; Pierini et al. 2003). Stacey et al. (1991) and Pierini et al. (1999) even considered the use of [CII] as a diagnostic for the SFR in non-starburst galaxies. Also Leech et al. (1999) found a correlation between [CII] emission and the star formation activity in an indirect way. They inferred a direct correlation of the [CII]-to-FIR flux ratio and [CII]-to-K'-band flux ratio with the galaxy lateness, which is correlated, in its turn, with massive star formation activity. Boselli et al. (2002) extended this analysis and calibrated the [CII] line flux as a star formation tracer based on $H\alpha$ + [NII] line fluxes. They found that the [CII] line intensity is not simply proportional to the star formation rate. Moreover, the scatter around the SFR calibration is considerable (an uncertainty of a factor ~ 10 when estimating the SFR from the [CII] line emission). Considering the recent improvement in techniques to deal with [NII] contamination (Decarli et al. 2007) and attenuation correction (Boselli et al. 2009) of $H\alpha$ data, we will extend the work done by Boselli et al. (2002) and provide a new calibration for the SFR relation based on other reliable star formation indicators. The sample in Boselli et al. (2002) consisted of 22 nearby late-type galaxies spanning a far-IR luminosity range of $10^8 \leq L_{\text{FIR}} \leq 10^{10.5} L_{\odot}$. We will extend this sample to more luminous galaxies up to $L_{\text{FIR}} \sim 10^{11.6} L_{\odot}$.

In case of normal star-forming late-type galaxies, a combination of indicators that trace the dust-enshrouded and unobscured star formation are able to give a complete picture of the star formation activity. Since UV radiation is mainly originating in massive young stars, it is an ideal tracer for the unobscured star formation. Solely relying on this unobscured fraction will underestimate the true star formation activity, as starburst regions are often affected by strong attenuation from surrounding interstellar dust clouds. To acquire a complete picture of the rate at which stars are formed, the dust-enshrouded star formation must be traced as well. The total amount of enshrouded star formation can be traced by the total IR-luminosity. But also several monochromatic SFR indicators have proven to be reliable estimators for the star formation activity. In particular, the mid-IR emission at 24 μm shows a general correlation with the star formation rate (Boselli, Lequeux & Gavazzi 2004; Calzetti et al. 2005; Wu et al. 2005; Alonso-Herrero et al. 2006; Pérez-González et al. 2006; Relaño et al. 2007; Calzetti et al. 2007; Bavouzet et al. 2008; Zhu et al. 2008; Rieke et al. 2009; Salim et al. 2009; Kennicutt et al. 2009).

In this paper, we investigate the correlation between [CII] luminosities and the SFR, estimated from the GALEX FUV and MIPS 24 μm or a combination of these SFR tracers. Based on the strength of these correlations, we will choose the SFR indicator showing the tightest correlation with [CII], which will serve as a reference SFR diagnostic in our analysis to calibrate the SFR-[CII] relation. §2 describes the sample selection and data acquisition. In §3, we estimate the SFR either from the monochromatic 24 μm luminosity or in combination with the GALEX FUV luminosity. Finally, §4 discusses the reliability and applicability of [CII] as a star formation rate indicator and also addresses the nature of [CII] emission in galaxies. §5 briefly summarizes our main conclusions.

2 SAMPLE AND DATA

2.1 Sample selection

The selection is based on the galaxy sample in Brauher et al. (2008), who assembled all galaxies with available [CII] data from the ISO archive. More specifically, we restrict our sample to those galaxies for which the [CII] line fluxes do not correspond to upper limits (i.e. non-detections) and which are classified in this paper as unresolved in the far-IR with respect to the $\sim 75''$ ISO LWS beam. This latter criterion implies that an aperture correction is not required for the [CII] line flux. Although a substantial fraction of the flux from an on-axis point source is diffracted out of the aperture beyond the diffraction limit at about 110 μm for all LWS detectors, these losses will be cancelled out in the calibration process, provided it is applied to point sources observed on-axis (Gry et al. 2003).

From this sample of 153 unresolved galaxies, we retain all galaxies that have been observed in both GALEX FUV and MIPS 24 μm bands, which gives us a final sample of 39 unresolved galaxies.

Some galaxies have multiple [CII] data, corresponding to apertures taken at different positions. For every galaxy, we only include one data point, preventing the introduction of any bias in our sample. If the different apertures show some overlap in area, we choose the aperture corresponding to the [CII] flux with the smallest uncertainty. If the overlap is insignificantly small, we add all fluxes from the apertures taken at different positions. The fluxes from the different apertures for the GALEX FUV and MIPS 24 μm are summed accordingly. This kind of flux summation has only been applied for two galaxies in our sample: NGC 4651 and NGC 7217.

Since FUV data are affected by galactic extinction, we have to apply appropriate corrections. At a galactic latitude $b = 11.^\circ 2$ (Clements 1983), NGC 1569 suffers from a large amount of Galactic extinction. Inconsistencies among the different reported estimates for the V-band extinction (e.g. $A_V = 1.79$ (Israel 1988); $A_V = 1.61$ (Devost et al. 1997); $A_V = 2.32$ (Schlegel et al. 1998)), made us decide to remove NGC 1569 from our sample, considering we want to avoid the introduction of any bias. This reduces our sample to 38 galaxies.

2.2 GALEX data

Far-ultraviolet (FUV, $\lambda = 1539 \text{ \AA}$, $\Delta\lambda = 442 \text{ \AA}$) observations of galaxies in our sample have been obtained from the GALEX GR4/5 public release. In order to derive accurate FUV photometry we only used fields with integration times greater than 800 sec, obtained as part of the Nearby Galaxy Survey, the Medium Imaging Survey or Guest Investigator programs (70 galaxies from our unresolved

sample of 153 galaxies have been observed by GALEX). We performed aperture photometry on the intensity maps produced by the standard GALEX pipeline. Details about the GALEX pipeline can be found in [Morrissey et al. \(2007\)](#). The GALEX FUV data have been corrected for galactic extinction according to [Schlegel et al. \(1998\)](#), using the extinction relation obtained from [Cardelli et al. \(1989\)](#).

2.3 MIPS 24 μ m data

The 24 micron images were created from raw data produced by the Multiband Imaging Photometer for Spitzer (MIPS; [Rieke et al. 2004](#)) on the Spitzer Space Telescope ([Werner et al. 2004](#)). The raw data were taken by a variety of programs using either the photometry mode (which produces 5 times 5 arcmin maps) or the scan map mode (which produces images that are typically 1 degree in length). We used the MIPS Data Analysis Tools ([Gordon et al. 2005](#)) along with additional processing steps to produce the final images. The individual data frames were processed through droop correction (to remove excess signal in each pixel proportional to the signal in the entire array), non-linearity correction, dark current subtraction, scan mirror position-dependent and position-independent flatfielding, and latent image removal steps. Background emission from the zodiacal light and additional scattered light that is related to the scan mirror position is then subtracted out. For objects observed in the scan map mode, the data from separate astronomical observation requests were used to make mosaics taken at individual epochs. These images were then subtracted from each other to identify asteroids, and the regions with asteroids were then masked out. Preliminary mosaics of each object were made using all data for each object to identify pixels in individual frames with values that are statistical outliers compared to other co-spatial pixels in other frames. These pixels were masked out, and then final mosaics were made using an image scale of 1.5 arcsec pixel⁻¹. Any residual background in the images was measured in multiple regions surrounding the optical disc and was then subtracted from the image. The final images are then calibrated using the conversion factor given by [Engelbracht et al. \(2007\)](#), which has an uncertainty of 4%. The FWHM of the PSF is 6 arcsec (Spitzer Science Center 2007).

2.4 Flux determination

We determine GALEX FUV and MIPS 24 μ m fluxes within the same aperture as the $\sim 75''$ ISO LWS beam. Variation in the shape of the point spread function used by the different instruments should not be an issue, as the necessary corrections have been applied through the calibration on a point source.

The GALEX FUV and MIPS 24 μ m fluxes were determined using the source-extracting code SExtractor ([Bertin & Arnouts 1996](#)). To align the apertures with the exact same position at which the [CII] fluxes were determined, we have created a fake object in IRAF (using the task mkobjects) at the same position coordinates of the actual pointing of the [CII] observation. Feeding SExtractor with this artificially created map and the FUV or 24 μ m image, assures us that the FUV and 24 μ m fluxes are extracted within the same area on the sky as the [CII] fluxes.

2.5 Spectral classification

Considering we will calibrate the [CII] luminosity against the SFR, derived either from the monochromatic 24 μ m flux or in combi-

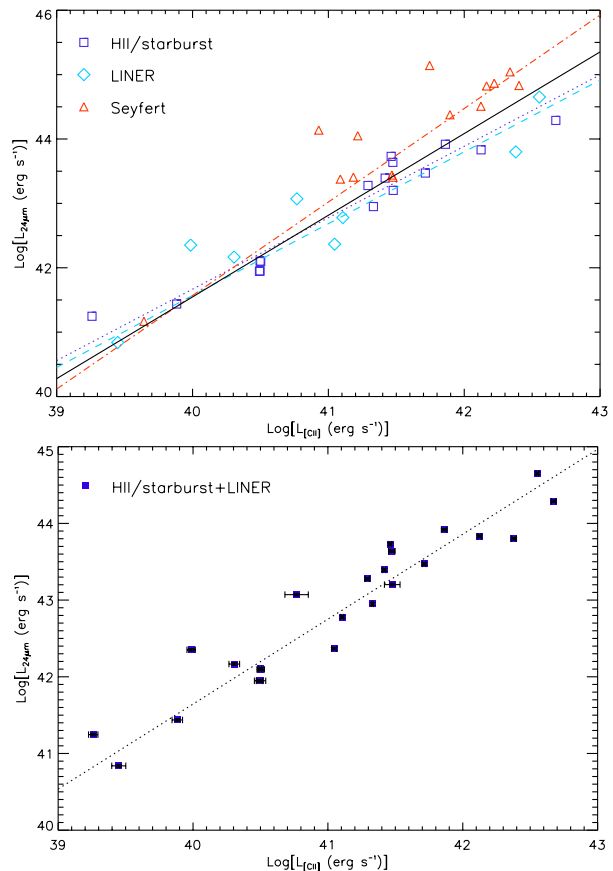


Figure 1. L_{CII} as a function of $L_{24\mu\text{m}}$. Upper panel: the three subsamples are represented (blue squares = HII/starburst, cyan diamond = LINER, red triangle = Sy1/Sy2). For reasons of clarity, we have omitted the errorbars from this plot. The best fitting line through the data points are indicated with a blue dotted, cyan dashed and red dashed-dotted line for the HII/starburst, LINER and Seyfert subsample, respectively. The mean trend for the complete sample is represented by a black solid line. The data points have a dispersion of 0.51 dex around this mean trend. Lower panel: the reduced sample, combining HII, starburst and LINER galaxies. The dotted line represents the best fitting line through the data points with a dispersion of 0.31 dex.

nation with the FUV flux, we have to make sure that the star-forming regions are the dominant contributor to this MIR emission. Therefore, we will classify our sample according to their nuclear spectral classification (see Table 1). We have made three different subdivisions. The first subgroup encompasses all objects resembling features typical of HII regions or starbursts. The second and third subset will include LINER and Seyfert galaxies, respectively. For this spectroscopic classification, we mainly rely on [Veron-Cetty & Véron \(2010\)](#), who have composed a compilation of AGN host galaxies. For the identification of the remaining sources and the objects with an uncertain classification in [Veron-Cetty & Véron \(2010\)](#), we have adopted the classification based on the optical spectra in [Veilleux et al. \(1995\)](#) and [Ho, Filippenko & Sargent \(1997\)](#), who both use similar selection criteria in their classification procedure. Additionally, for some sources we used the classification from [Veron-Cetty & Veron \(1986\)](#). Considering that the optical spectroscopic classification for FIR-luminous objects not always offers a clear distinction between starburst- or AGN-dominated nuclear activity, we additionally examine spectroscopic L-band data ([Risaliti 2004](#)) and radio properties ([Baan](#)

& Klöckner 2006), if available for those objects. Based on several L-band diagnostics, Risaliti (2004) found a dominant AGN-contribution to the energy output in the infrared for IRAS 19254-7245, IRAS 20551-4250 and one of the two optical nuclei in IRAS 23128-5919. Baan & Klöckner (2006) found from their radio observations that an AGN is the dominant power source in the nucleus of CGCG1510.8+0725. Four sources remain unclassified, but since they all host HII regions (Cartwheel: Gao et al. 2003, NGC1317: Crocker et al. 1996, NGC 4189 and NGC 4299: Hodge & Kennicutt 1983), we assign them to the HII/starburst group.

Our sample of 38 galaxies contains 16 galaxies for which HII regions or starbursts dominate their central regions, while the remaining sources in our sample are host galaxies of an AGN (14 galaxies) or LINER (8 galaxies). For these different nuclear regimes, we will examine the power sources that mainly contribute to the 24 μ m emission. Plotting $L_{\text{[CII]}}$ as a function of the MIPS 24 μ m luminosity for the three different subsets, we immediately deduce a significant contribution from the AGN in Seyfert galaxies to the 24 μ m emission (see the upper panels in Figure 1). The dispersion around the mean trend for the complete sample of galaxies is 0.51 dex in Figure 1. For galaxies classified as a LINER, starbursts appear to be the main power supply for the MIPS 24 μ m. Although the spectral line emission in some LINERs might also be generated by a quiescent AGN, this contribution does not appear to be significant for the LINER galaxies in our sample. Because of the insignificant AGN contribution to the MIR emission in LINERs, we perform our calibration analysis on a reduced sample that combines the two subsets (HII regions, starbursts and LINERs), which all have a dominant contribution from starburst to the MIR emission. This final sample consists of 24 galaxies of which 16 show features of HII regions and 8 other galaxies are classified as a LINER. Plotting again the same correlations for this final sample (see Figure 1, bottom panel), we can quantify that most of the scatter in previous plots was due to the contribution of an AGN to the 24 μ m emission. Indeed, the dispersion around the mean trend reduces to 0.31 dex in Figure 1 (bottom panel).

2.6 Sample description

The galaxies in our final sample span a range of almost 4 orders of magnitude in total infrared luminosity (L_{TIR}), from $\sim 1.2 \times 10^{42}$ to $\sim 2.7 \times 10^{45}$ erg s $^{-1}$ (L_{TIR} was calculated based on equation (5) in Dale & Helou 2002, relying on the IRAS 25, 60 and 100 μ m fluxes). In this final sample of 24 galaxies (HII regions, starbursts and LINERs), five galaxies are classified as LIRG ($L_{\text{TIR}} > 10^{11} L_{\odot}$). Figure 2 demonstrates this wide range in L_{TIR} and shows its dependence on the $f_{\nu}(60\mu\text{m})$ -to- $f_{\nu}(100\mu\text{m})$ ratio, which is a proxy for the effective dust temperature. As most galaxies in our sample have high effective temperatures, the IRAS 100 μ m flux samples the SED peak of dust emission rather well. This was also confirmed by Kennicutt et al. (2009), as they found that the IRAS fluxes give a reliable representation of the total infrared luminosity for galaxies obeying $f_{\nu}(60\mu\text{m})/f_{\nu}(100\mu\text{m}) > 0.4$. Only six galaxies in our sample have a $f_{\nu}(60\mu\text{m})$ -to- $f_{\nu}(100\mu\text{m})$ ratio below this value.

Our sample covers a large range in distance, going from 3.9 to 139.1 Mpc. Four galaxies (NGC 4189, NGC 4293, NGC 4299 and NGC 7714) are in common with the sample that was used in Boselli et al. (2002).

Table 1 gives an overview of all relevant information for our sample galaxies. We arranged their properties as follow:

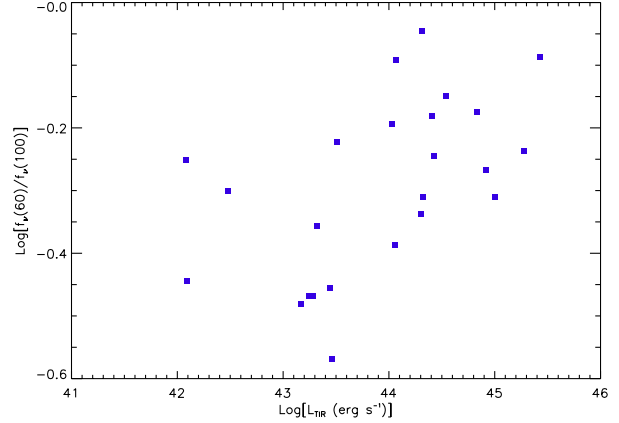


Figure 2. The ratio $f_{\nu}(60\mu\text{m})$ -to- $f_{\nu}(100\mu\text{m})$, which is a proxy for the effective dust temperature, as a function of the total infrared luminosity L_{TIR} .

- Column 1: galaxy name, NGC, IC, CGCG, UGC or IRAS, for the sample galaxies.
- Column 2: distance [Mpc], derived from the Nearby Galaxies Catalogue (Tully 1988) and for other galaxies, from their recession velocity (from NED) assuming $H_0 = 70$ km s $^{-1}$ Mpc $^{-1}$.
- Column 3: morphological type, adopted from de Vaucouleurs et al. (1991).
- Column 4, 5: classification of the nuclear spectrum: HII or starburst, LINER, Seyfert (1 or 2), and the corresponding references for this classification.
- Column 6: $f_{\nu}(60\mu\text{m})$ -to- $f_{\nu}(100\mu\text{m})$ ratio of the IRAS fluxes, a proxy for the effective dust temperature.
- Column 7: Total-IR luminosity [erg/s] for the whole galaxy, as calculated from equation (5) in Dale & Helou (2002).

Table 2 summarizes all relevant published data and measured fluxes within the $\sim 75''$ ISO LWS beam for the analysis in this paper. Summing up:

- Column 1: galaxy name, NGC, IC, CGCG, UGC or IRAS, for the sample galaxies.
- Column 2, 3: Actual pointing position: right ascension (RA) and declination (DEC) from the [CII] observation, both in decimal degrees (from Brauer et al. 2008).
- Column 4: [CII] line flux, in [fW/m 2], and the uncertainty on this flux measurement (from Brauer et al. 2008).
- Column 5: GALEX FUV flux, [mJy], and the corresponding uncertainty. Both values have been corrected for galactic extinction, according to Schlegel et al. (1998) and Cardelli et al. (1989).
- Column 6: Spitzer MIPS 24 μ m flux, [mJy], and the corresponding uncertainty, including both uncertainties in the flux extraction ($< 2\%$) and the calibration (4%, Engelbracht et al. 2007).

Although this final sample of 24 galaxies, gathering objects classified as HII region, starburst or LINER, is neither statistically significant nor representative for the whole of galaxies with diverging properties, this sample enables us to make a first preliminary analysis of the diagnostic capabilities of [CII] in tracing the star formation activity in galaxies. For a thorough analysis based on a more extensive sample of galaxies, we will have to wait until the completion of all [CII] surveys with the Herschel Space Observatory. Nevertheless, the broad range of optical and infrared luminosities covered in our sample enables us to infer the reliability of [CII] as a star formation indicator in star-forming galaxies spanning almost 4 orders of magnitude.

Table 1. Properties for the galaxies in our sample.

Name	Distance (Mpc)	Type ¹	Spectral type	Ref ²	IRAS 60 / IRAS 100	log L_{TIR} log (erg/s)
(1)	(2)	(3)	(4)	(5)	(6)	(7)
Cartwheel	129.3	RING	HII/sb	no ³	0.46	44.30
NGC 0520	27.8	Pec	HII/sb	3	0.66	44.41
NGC 0625	3.9	SB(s)m? edge-on	HII/sb	1	0.56	42.08
NGC 0660	11.8	SB(s)a pec	LINER	1, 2, 3	0.64	44.03
NGC 0695	139.1	S0? pec	HII/sb	2	0.58	45.28
NGC 0986	23.2	SB(rs ab	HII/sb	4	0.49	44.32
UGC 02238	92.3	Im?	LINER	2	0.54	44.92
NGC 1156	6.4	IB(s)m	HII/sb	3	0.50	42.48
NGC 1266	31.3	(R') SB(rs) 0 \wedge 0 pec:	LINER	1, 2	0.81	44.07
NGC 1275	75.2	Pec	Seyfert	1, 3	1.02	44.49
NGC 1317	16.9	SAB(r)a	HII/sb	no	0.34	43.28
NGC 1569	1.6	IBm	HII/sb	3	0.98	42.15
IRAS 05189-2524	182.3		Seyfert	1, 2	1.20	45.74
UGC 03426	57.9	S0:	Seyfert	1	1.12	44.58
NGC 2388	59.1	S?	HII/sb	2	0.67	44.83
NGC 4041	22.7	SA(rs)bc:	HII/sb	3	0.41	44.06
NGC 4189	16.8	SAB(rs) cd?	HII/sb	no	0.34	43.24
NGC 4278	9.7	E1-2	LINER	3	0.36	42.09
NGC 4293	17.0	(R) SB(s) 0/a	LINER	3	0.44	43.32
NGC 4299	16.8	SAB(s)dm:	HII/sb	no	0.33	43.17
NGC 4490	7.8	SB(s)d pec	HII/sb	3	0.60	43.51
NGC 4651	16.8	SA(rs)c	LINER	3	0.35	43.44
NGC 4698	16.8	SA(s)ab	Seyfert	1, 3	0.31	42.65
IC 4329A	68.8	SA0 \wedge +: edge-on	Seyfert	1	1.22	44.59
NGC 5713	30.4	SAB(rs)bc pec	HII/sb	4	0.57	44.43
CGCG 1510.8+0725	55.7		Seyfert	6	0.66	44.76
NGC 6221	19.4	SB(s)c	Seyfert	1	0.50	44.37
NGC 6240	104.8	I0: pec	LINER	1, 2	0.82	45.43
IRAS 19254-7245	264.3		Seyfert	1, 5	0.95	45.68
NGC 6810	25.3	SA(s)ab:	Seyfert	4	0.52	44.28
IRAS 20551-4250	184.1		Seyfert	1, 5 ⁴	1.29	45.55
NGC 7217	16.0	(R)SA(r)ab	LINER	1, 3	0.27	43.46
NGC 7469	69.9	(R')SAB(rs)a	Seyfert	1, 2	0.74	45.25
IRAS 23128-5919	191.0		Seyfert	1, 5 ⁵	0.98	45.58
NGC 7552	19.5	(R')SB(s)ab	HII/sb	1	0.71	44.54
NGC 7582	17.6	(R')SB(s)ab	Seyfert	1	0.67	44.25
NGC 7714	36.9	SB(s)b: pec	HII/sb	1, 2	0.90	44.31
IRASF23365+3604	276.2		Seyfert	1	0.84	45.74
NGC 7771	61.1	SB(s)b: pec	HII/sb	2	0.49	45.00

¹ The galaxy type has been adopted from [de Vaucouleurs et al. \(1991\)](#). If no galaxy type is mentioned, there was no classification available in the literature.² The references of the spectral type: 1: [Veron-Cetty & Véron \(2010\)](#); 2: [Veilleux et al. \(1995\)](#); 3: [Ho, Filippenko & Sargent \(1997\)](#); 4: [Veron-Cetty & Veron \(1986\)](#); 5: [Risaliti \(2004\)](#) 6: [Baan & Klöckner \(2006\)](#)³ "no" indicates that no classification was found in the literature. These objects were classified in the HII/starburst group based on detected HII regions in their nuclei. Section 2.5 discusses the classification for these galaxies more into detail.⁴ Based on optical spectra IRAS 20551-4250 was classified as a starburst galaxy ([Veron-Cetty & Véron 2010](#)), but according to L-band diagnostics a significant AGN contribution is present ([Risaliti 2004](#)).⁵ This galaxy has a pair of optical nuclei, which is probably a remnant of a merging process. [Veron-Cetty & Véron \(2010\)](#) identified this galaxy as HII region, while [Risaliti \(2004\)](#) reported that one nucleus shows AGN features and the other nucleus resembles a HII region. Since both nuclei fall within the ISO LWS beam, we have classified this object as a Seyfert galaxy, based on the AGN-contribution from at least one nucleus.

3 RELIABLE REFERENCE SFR TRACER

In order to compare the different star formation relations, it is important that they are calibrated in the same way. Therefore we will relate all relations to the same initial mass function (IMF). This reference IMF will be the [Kroupa \(2001\)](#) IMF, characterized by a power law $\xi(m) \propto m^{-\alpha}$ with slope $\alpha = 2.3$ for 0.5-100 M_{\odot} and $\alpha =$

1.3 for 0.1-0.5 M_{\odot} . We prefer the [Kroupa \(2001\)](#) IMF rather than the more commonly used [Salpeter \(1955\)](#) IMF (with a single slope $\alpha = 2.35$ for 0.1-100 M_{\odot}), since the former better correlates with IMF observations in the Galactic field ([Chabrier 2003](#); [Kroupa & Weidner 2003](#)).

Analyzing the correlations between $L_{\text{[CII]}}$ and the SFR requires a complete threefold approach:

Table 2. Sample galaxies: data

Name	RA	DEC	[CII]	GALEX FUV	MIPS 24
(1)	(deg)	(deg)	(fW/m ²)	(mJy)	(mJy)
(1)	(2)	(3)	(4)	(5)	(6)
Cartwheel	9.4171	-33.7239	0.15 ± 0.02	1.980 ± 0.009	63.7 ± 2.7
NGC 0520	21.1458	+3.7950	2.83 ± 0.07	0.787 ± 0.009	2139.3 ± 85.7
NGC 0625	23.7799	-41.4357	1.00 ± 0.08	8.239 ± 0.016	776.0 ± 31.2
NGC 0660	25.7595	+13.6458	7.67 ± 0.19	0.386 ± 0.007	2889.9 ± 115.7
NGC 0695	27.8091	+22.5825	2.04 ± 0.08	3.869 ± 0.003	672.4 ± 27.0
NGC 0986	38.3922	-39.0462	3.04 ± 0.11	0.964 ± 0.011	2355.9 ± 94.4
UGC 02238	41.5726	+13.0958	2.35 ± 0.09	0.448 ± 0.012	496.2 ± 20.0
NGC 1156	44.9271	+25.2375	1.56 ± 0.14	23.307 ± 0.115	447.1 ± 18.0
NGC 1266	49.0032	-2.4271	0.50 ± 0.10	0.216 ± 0.009	804.1 ± 32.3
NGC 1275	49.9525	+41.5105	1.16 ± 0.07	4.766 ± 0.014	2814.7 ± 112.7
NGC 1317	50.6862	-37.1027	0.91 ± 0.05	1.974 ± 0.013	207.2 ± 8.4
NGC 1569	67.7046	+64.8478	5.99 ± 0.16	105.217 ± 0.314	6495.8 ± 260.0
IRAS 05189-2524	80.2558	-25.3624	0.14 ± 0.02	0.126 ± 0.004	2786.6 ± 111.6
UGC 03426	93.9016	+71.0376	0.41 ± 0.02	0.662 ± 0.020	2238.1 ± 89.7
NGC 2388	112.2229	+33.8182	1.74 ± 0.08	0.135 ± 0.005	1585.2 ± 63.5
NGC 4041	180.5501	+62.1363	3.48 ± 0.05	1.880 ± 0.001	1159.7 ± 46.5
NGC 4189	183.4465	+13.4240	0.94 ± 0.06	2.243 ± 0.001	295.7 ± 12.0
NGC 4278	185.0276	+29.2824	0.25 ± 0.03	0.883 ± 0.010	49.1 ± 2.1
NGC 4293	185.3050	+18.3844	0.28 ± 0.02	0.111 ± 0.003	520.1 ± 20.9
NGC 4299	185.4189	+11.5012	0.93 ± 0.09	8.996 ± 0.030	210.4 ± 8.5
NGC 4490	187.6536	+41.6398	4.32 ± 0.11	10.248 ± 0.022	1394.8 ± 55.9
NGC 4651	190.9271	+16.3942	2.03 ± 0.08	4.048 ± 0.015	383.1 ± 15.5
NGC 4651	190.9442	+16.3972	0.50 ± 0.06	1.533 ± 0.010	79.6 ± 3.3
NGC 4651	190.91	+16.3914	0.76 ± 0.09	1.732 ± 0.010	88.0 ± 3.6
NGC 4651	total from all positions		3.29 ± 0.13	7.314 ± 0.021	550.7 ± 22.2
NGC 4698	192.0969	+8.4875	0.13 ± 0.02	0.289 ± 0.004	34.9 ± 1.5
IC 4329A	207.3304	-30.3095	0.15 ± 0.02	0.073 ± 0.003	1945.3 ± 77.9
NGC 5713	220.0478	-0.2905	4.68 ± 0.13	4.061 ± 0.020	2144.6 ± 85.9
CGCG 1510.8+0725	228.3053	+7.2265	0.33 ± 0.05	0.086 ± 0.004	514.3 ± 20.7
NGC 6221	253.1913	-59.2167	6.64 ± 0.25	4.527 ± 0.063	4528.1 ± 181.3
NGC 6240	253.2450	+2.4013	2.72 ± 0.06	0.637 ± 0.004	2735.4 ± 109.5
IRAS 19254-7245	292.8400	-72.6319	0.26 ± 0.07	0.162 ± 0.005	1059.0 ± 42.5
NGC 6810	295.8915	-58.6556	3.83 ± 0.13	0.553 ± 0.010	2882.1 ± 115.4
IRAS 20551-4250	314.6116	-42.6518	0.41 ± 0.03	0.600 ± 0.006	1450.9 ± 58.2
NGC 7217	331.9775	+31.35833	0.66 ± 0.06	1.557 ± 0.008	197.9 ± 8.0
NGC 7217	331.95833	+31.35972	0.62 ± 0.07	1.331 ± 0.008	185.2 ± 7.5
NGC 7217	total from all positions		1.28 ± 0.09	2.888 ± 0.012	383.1 ± 15.5
NGC 7469	345.81417	+8.87361	2.27 ± 0.03	6.963 ± 0.020	4421.9 ± 177.0
IRAS 23128-5919	348.9454	-59.0544	0.58 ± 0.05	0.557 ± 0.005	1242.2 ± 49.8
NGC 7552	349.045	-42.5844	6.37 ± 0.15	3.746 ± 0.011	9443.8 ± 377.9
NGC 7582	349.5988	-42.3703	4.12 ± 0.13	0.900 ± 0.006	5516.4 ± 220.8
NGC 7714	354.0612	+2.1550	1.83 ± 0.10	7.893 ± 0.018	2131.7 ± 85.4
IRASF23365+3604	354.7554	+36.3528	0.16 ± 0.02	0.197 ± 0.006	585.2 ± 23.5
NGC 7771	357.8534	+20.1119	2.98 ± 0.09	0.906 ± 0.012	1216.5 ± 48.8

• We first analyze the simple relation of the SFR as a function of the [CII] luminosity. Although this approach is most straightforward, the data might be biased towards larger distances. Since the distances to the galaxies in our sample range from 3.9 to 139.1 Mpc, we have to eliminate the distance bias in this luminosity versus luminosity relation.

• Plotting $\text{SFR}/4\pi D^2$ as a function of the [CII] flux, the distance bias is removed. If a true [CII]-SFR correlation is present, it will be confirmed in this plot.

• The dispersion around the mean trend is best quantified in a plot of the [CII] luminosity versus the residual of the best fitting relation between $L_{[\text{CII}]}$ and the SFR. The SFR relation showing the

tightest correlation with the [CII] luminosity will be characterized by the lowest dispersion in the residual plots.

3.1 SFR calibrated against TIR

Taking into account that the 24 μm emission from a galaxy better correlates with the SFR as opposed to monochromatic FIR measurements at longer wavelengths (70 and 160 μm) (Calzetti et al. 2010), we have only estimated the SFR, which is used for the final calibration of the SFR-[CII] relation, from 24 μm data (or FUV luminosities which have been corrected for attenuation based on 24 μm data) in this work. To obtain a second independent SFR di-

agnostic, we have investigated whether TIR luminosities for these galaxies could be used as a calibrator. Since we only have IRAS fluxes covering the whole galaxy for all sample objects to estimate the TIR luminosity, we checked whether an aperture correction was required. Although the galaxies in our sample were selected based on the criterion that they are unresolved in the FIR with respect to the *ISO* LWS beam, many of them are resolved within the *ISO* beam in optical data. Therefore, we visually inspected the MIPS $24\mu\text{m}$ images and could indeed quantify that also in the MIR a significant fraction of the total flux for several galaxies fell outside the *ISO* beam aperture. Subsequently, we verified the availability of MIPS 70 and $160\mu\text{m}$ data in the Spitzer archive, to determine the correct TIR luminosities which correspond to the portion of the flux that falls within the same *ISO* beam. Considering that only 28 of the 38 sample galaxies have full coverage in all Spitzer bands, and some of those galaxies were only observed in small fields which does not allow proper convolution with the appropriate kernel to match the PSF's in all Spitzer bands, we decided not to use these Spitzer data. Moreover, the varying sizes of the sample galaxies would imply a different aperture correction (some are point sources and others are clearly more extended), introducing an additional bias to the TIR luminosity derived from these Spitzer data. While the MIPS $24\mu\text{m}$ clearly demonstrate that the majority of our sample galaxies requires some kind of aperture correction, we have verified that the data currently at hand are not able to properly correct for these aperture issues. Any empirical correction can significantly bias the correlations between the [CII] luminosity and the SFR derived from this aperture-corrected TIR luminosity and does not allow us to draw any firm conclusion. Therefore, this paper only investigates the correlation between [CII] and the SFR, when estimated from the $24\mu\text{m}$ or attenuation-corrected FUV flux.

3.2 SFR calibrated against MIPS $24\mu\text{m}$

In this section, we predict the star formation rate solely relying on the MIR emission at $24\mu\text{m}$, to trace the dust-enshrouded fraction of star formation.

First, we have to choose an appropriate star formation relation. Several SFR relations based on $24\mu\text{m}$ emission have been published. Some authors claim a linear relation between the SFR and $L_{24\mu\text{m}}$ (Wu et al. 2005; Zhu et al. 2008), while others argue that only a non-linear relation can account for the increasing $24\mu\text{m}$ emission in more IR-luminous galaxies which form stars at a higher rate (Wu et al. 2005; Pérez-González et al. 2006; Alonso-Herrero et al. 2006; Calzetti et al. 2007; Relaño et al. 2007; Zhu et al. 2008; Rieke et al. 2009; Boquien et al. 2010). As some galaxies in our sample are situated at the high luminosity end, we should be aware that this non-linear effect might affect our results. We choose to estimate the SFR from the relation in Rieke et al. (2009).

Rieke et al. (2009) use a combination of a linear trend at lower TIR luminosities and a non-linear relation above a threshold of $L_{\text{TIR}} > 10^{11} L_{\odot}$ or $L_{24\mu\text{m}} > 1.3 \times 10^{10} L_{\odot}$. Both relations were derived from a sample of dusty, luminous star-forming galaxies and hold up to $L_{\text{TIR}} = 2 \times 10^{12} L_{\odot}$, which is higher than the most luminous galaxy in our sample (NGC 6240; $7.0 \times 10^{11} L_{\odot}$). The overlap between our range in TIR luminosities and the similar characteristics of both samples make us confident that this relation gives a good indication of the true star formation rate in our sample galaxies. The two relations from Rieke et al. (2009) are (assuming our reference Kroupa 2001 IMF):

$$\text{SFR} = 2.04 \times 10^{-43} L_{24\mu\text{m}} \quad (1)$$

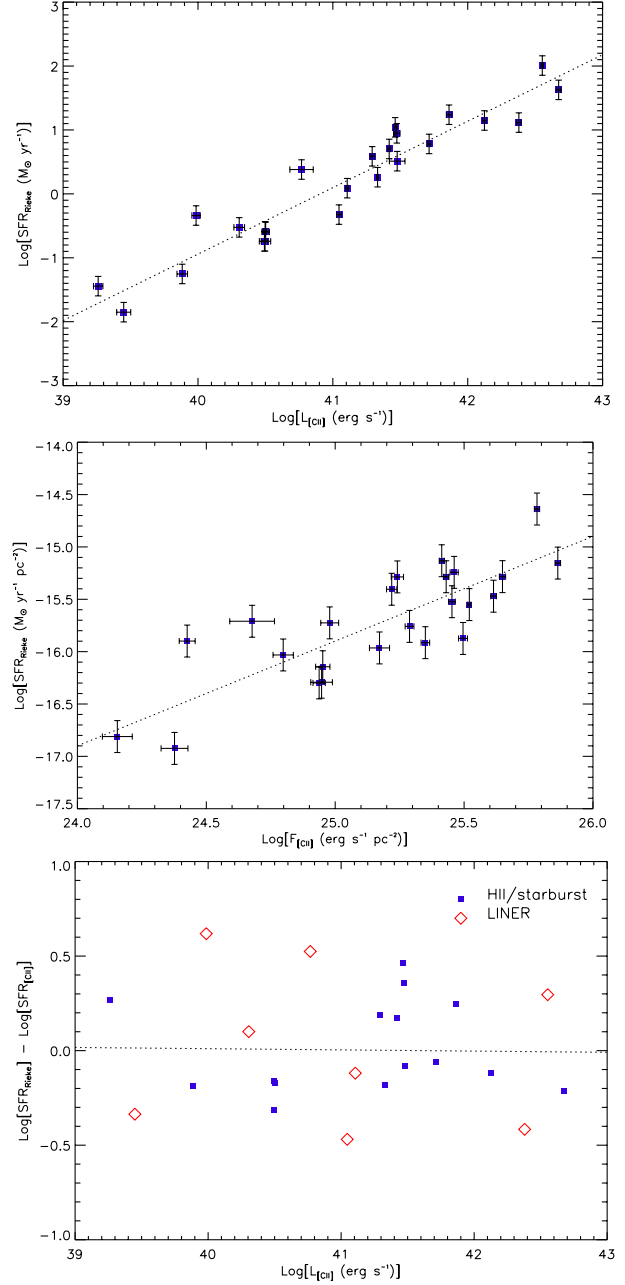


Figure 3. Upper panel: $\text{SFR}_{24\mu\text{m}}$ (SFR relation from Rieke et al. (2009)) as a function of L_{CII} , central panel: $\text{SFR}_{24\mu\text{m}}/4\pi D^2$ as a function of [CII] flux, bottom panel: residuals of the $\text{SFR}_{24\mu\text{m}}-L_{\text{CII}}$ plot. In this residual plot, HII/starburst and LINER galaxies are indicated as blue filled squares and red diamonds, respectively.

for $4 \times 10^{42} \lesssim L_{24\mu\text{m}} \lesssim 5 \times 10^{43} \text{ erg s}^{-1}$ and

$$\text{SFR} = 2.04 \times 10^{-43} \times L_{24\mu\text{m}} (2.03 \times 10^{-44} L_{24\mu\text{m}})^{0.048} \quad (2)$$

for $L_{24\mu\text{m}} > 5 \times 10^{43} \text{ erg s}^{-1}$, where SFR and $L_{24\mu\text{m}}$ have units $\text{M}_{\odot} \text{ yr}^{-1}$ and erg s^{-1} , respectively.

After estimating the SFR from these relations, we verify the strength of the correlation between L_{CII} and the SFR through a three-pronged approach. First, we plot the derived SFR as a function of L_{CII} (see Figure 3, upper panel). The best fitting line

through the data points corresponds to:

$$\log \text{SFR}_{24\mu\text{m}} = 1.040 \log L_{[\text{CII}]} - 42.535 \quad (3)$$

where the units of $\text{SFR}_{24\mu\text{m}}$ and $L_{[\text{CII}]}$ are in $M_{\odot} \text{ yr}^{-1}$ and erg s^{-1} , respectively. The 1σ dispersion of the individual galaxies around the best fitting line is 0.30 dex. This 1σ dispersion has been calculated as the standard deviation of the logarithmic distance from the data points to the best fitting line weighted by the error on the individual quantities. Since the observed trend in this plot of luminosity versus SFR (and thus indirectly luminosity) might be biased by the range in distances among our sample galaxies, we remove this distance bias in the central panel of Figure 3. In this figure, we plot the $\text{SFR-to-}4\pi D^2$ ratio as a function of the $[\text{CII}]$ flux. Since this distance-independent plot still shows a similar correlation between $[\text{CII}]$ and the SFR and the dispersion 0.30 dex is of the same order as in the first panel, we safely conclude that the observed correlation in the upper panel of Figure 3 is not due to a distance bias in the data set. The dispersion around the mean trend (see Equation 3) is better represented in the bottom panel of Figure 3, which shows the residual plot.

3.3 SFR calibrated against GALEX FUV + MIPS 24 μm

Before the GALEX FUV flux can be used as a direct quantifier of the star formation activity in a galaxy, a correction for internal dust attenuation has to be applied. The specific amount of extinction that is affecting the UV light is difficult to quantify, because different galaxies will be characterized by different extinction laws and a variation of stellar and dust distributions. In this section, we will rely on SFR relations that use a combination of the GALEX FUV flux and the monochromatic MIR emission at $24\mu\text{m}$ to obtain a complete picture of the star formation activity.

Two SFR relations have been reported, making use of both photometric data. First, [Zhu et al. \(2008\)](#) derived a linear relation to estimate the attenuation-corrected FUV-flux based on the observed FUV and $24\mu\text{m}$ data:

$$L_{\text{FUV,corr}}[L_{\odot}] = L_{\text{FUV,obs}}[L_{\odot}] + 6.31 L_{24\mu\text{m}}[L_{\odot}]. \quad (4)$$

For the derivation of this relation, [Zhu et al. \(2008\)](#) relied on a sample of 187 star-forming (non-AGN) galaxies.

Another relation, reported in [Leroy et al. \(2008\)](#), also computes the SFR from both FUV and $24\mu\text{m}$ data. Since a large fraction of our sample galaxies are characterized by a much higher star formation activity with respect to the sample in [Leroy et al. \(2008\)](#), we will apply the attenuation correction as reported in [Zhu et al. \(2008\)](#) and rely on the SFR relation in [Kennicutt et al. \(2009\)](#):

$$\text{SFR} = 0.88 \times 10^{-28} L_{\text{FUV,corr}}, \quad (5)$$

where the units of $L_{\text{FUV,corr}}$ are in $\text{erg s}^{-1} \text{ Hz}^{-1}$, to derive a star formation rate from the extinction-corrected FUV data. This relation was derived for a sample of normal galaxies in the present-day universe and most star-forming galaxies out to redshifts $z \sim 1$. With an upper limit of $\log L_{\text{TIR}}[L_{\odot}] \sim 11.9$, the relation is not immediately representative for the most dust-obscured LIRGs or ULIRGs found in the present-day universe (but this is not applicable for galaxies in our non AGN-dominated sample).

Figure 4 shows the correlation between $L_{[\text{CII}]}$ and the $\text{SFR}_{\text{FUV}+24\mu\text{m}}$ derived in this way. The best fitting line through all data points is given by:

$$\log \text{SFR}_{\text{FUV}+24\mu\text{m}} = 0.983 \log L_{[\text{CII}]} - 40.012 \quad (6)$$

where the units of $\text{SFR}_{\text{FUV}+24\mu\text{m}}$ and $L_{[\text{CII}]}$ are in $M_{\odot} \text{ yr}^{-1}$ and erg s^{-1} ,

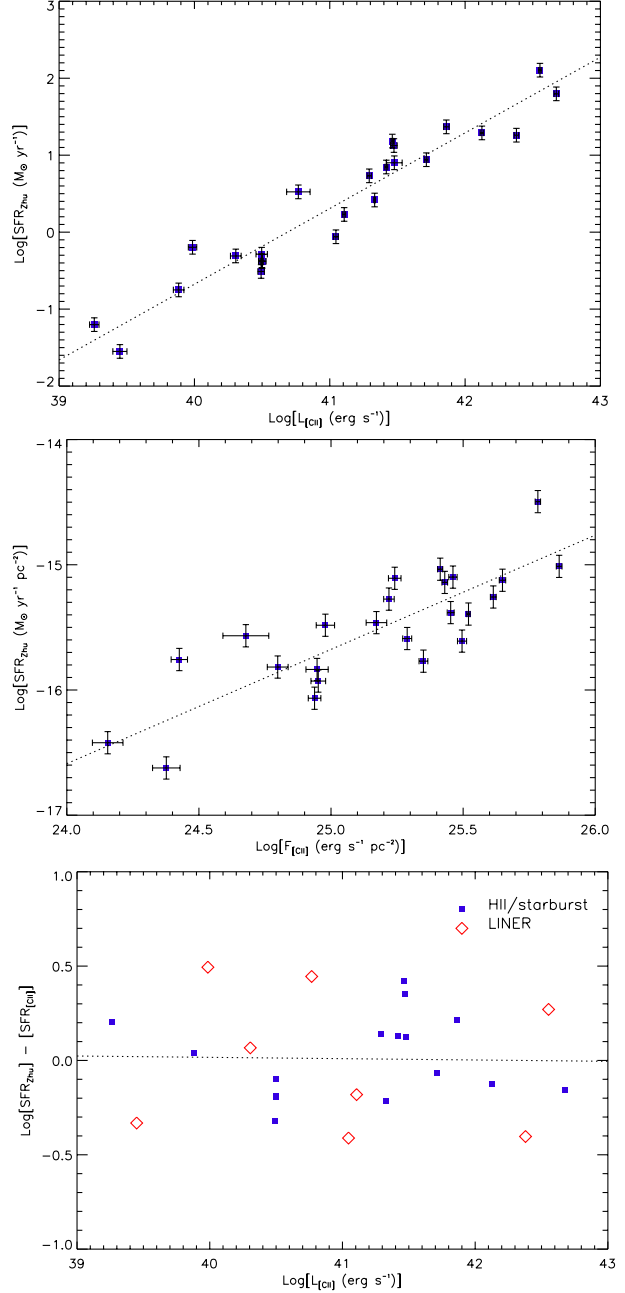


Figure 4. $\text{SFR}_{\text{FUV}+24\mu\text{m}}$ (attenuation correction and SFR relation from [Zhu et al. \(2008\)](#) and [Kennicutt et al. \(2009\)](#), respectively) as a function of $L_{[\text{CII}]}$, central panel: $\text{SFR}_{\text{FUV}+24\mu\text{m}}/4\pi D^2$ as a function of $[\text{CII}]$ flux, bottom panel: residuals of the $\text{SFR}_{\text{FUV}+24\mu\text{m}}-L_{[\text{CII}]}$ plot. In this residual plot, HII/starburst and LINER galaxies are indicated as blue filled squares and red diamonds, respectively.

respectively. The spread around the mean trend is represented in the bottom panel of Figure 4 and can be quantified by a 1σ dispersion of 0.27 dex. The central panel of Figure 4 again confirms that the observed trend is not due to a distance bias in our sample, since the 1σ spread around the mean trend (0.26 dex) does not differ in this distance independent relation.

Relying on the relation in [Zhu et al. \(2008\)](#), we can quantify the fraction of dust-enshrouded and unobscured star formation. Figure 5 plots the ratio between the observed FUV luminosity and

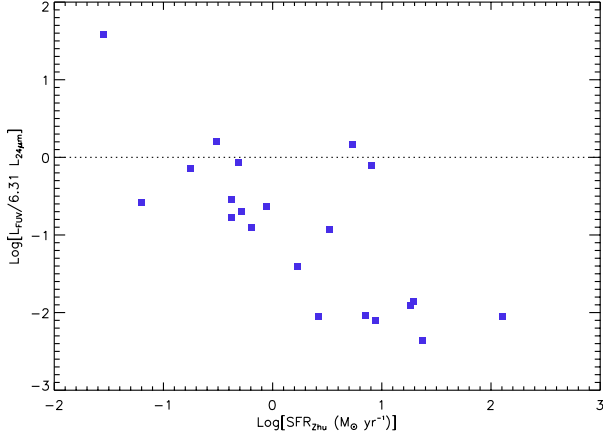


Figure 5. The ratio $L_{\text{FUV}} / 6.31 L_{24\mu\text{m}}$ as a function of the total SFR, as derived from formula 4 and 5. This ratio of luminosities represents the fraction of unobscured star formation. The factor α in the denominator is the proportionality factor adopted from [Zhu et al. \(2008\)](#). For $\alpha = 6.31$, they found that the sum $L_{\text{FUV,obs}} + 6.31 L_{24\mu\text{m}}$ is a good approximation of the attenuation corrected FUV flux.

the scaled MIPS $24\mu\text{m}$ luminosity, for which the scaling coefficient $\alpha = 6.31$ was adopted from [Zhu et al. \(2008\)](#), as a function of the SFR. This $L_{\text{FUV}}/\alpha L_{24\mu\text{m}}$ ratio represents the unobscured fraction of star formation. Figure 5 illustrates that the majority of our sample galaxies have a dominant contribution to the $24\mu\text{m}$ emission from dust grains heated by a young stellar population, rather than direct FUV emission from young stars. This makes the $24\mu\text{m}$ or a combination of GALEX FUV data and an appropriate attenuation correction a more reliable star formation indicator for our sample than solely relying on UV data. One exception is NGC 4278, for which the unobscured fraction of star formation dominates dust-enshrouded $24\mu\text{m}$ emission of young stellar objects. Furthermore, Figure 5 shows a hint for a decreasing trend in the unobscured fraction of star formation towards higher SFR. This trend can be accounted for by an increasing opacity for galaxies which form stars at a higher rate.

4 DISCUSSION

4.1 [CII] as a SFR indicator

In the previous section, we found that the star formation rate correlates well with the [CII] luminosity. Table 3 summarizes the star formation rates obtained from the two different star formation relations for all galaxies in our reduced sample. Table 4 summarizes the coefficients a and b for the best fitting line $y = ax + b$ for each star formation tracer, the uncertainty on the slope a and intercept b and the 1σ dispersion of the individual galaxies around this mean trend. For both star formation relations, the uncertainties on the slope and intercept of the best fitting line are small and the spread around the mean trend is narrow. The dispersion around the correlation is smaller for the SFR derived from a combination of GALEX FUV and $24\mu\text{m}$ data (0.27 dex), than when estimating the SFR from the single $24\mu\text{m}$ luminosities (0.30 dex) (see also the bottom panels of Figures 3 and 4). Considering that a combination of FUV and $24\mu\text{m}$ data traces the complete star formation activity, as opposed to the single $24\mu\text{m}$ data, which only traces the obscured fraction of star formation, we will use the SFR tracing both the dust-enshrouded and unobscured activity to calibrate the SFR relation. Since the dis-

Table 3. Star formation rates for the galaxies in our sample, derived from different SFR relations based on MIPS $24\mu\text{m}$ data, or a combination of GALEX FUV with MIPS $24\mu\text{m}$ data.

Name	Rieke2009 ($M_{\odot} \text{ yr}^{-1}$)	Zhu2008+Kennicutt2009 ($M_{\odot} \text{ yr}^{-1}$)
(1)	(2)	(3)
Cartwheel	3.25 ± 1.14	7.97 ± 1.63
NGC 0520	5.04 ± 1.77	7.02 ± 1.43
NGC 0625	0.04 ± 0.01	0.06 ± 0.01
NGC 0660	1.23 ± 0.43	1.70 ± 0.35
NGC 0695	42.37 ± 14.88	62.63 ± 12.78
NGC 0986	3.87 ± 1.36	5.39 ± 1.10
UGC 02238	13.04 ± 4.58	18.19 ± 3.72
NGC 1156	0.06 ± 0.02	0.18 ± 0.04
NGC 1266	2.40 ± 0.84	3.34 ± 0.68
NGC 1317	0.18 ± 0.06	0.31 ± 0.06
NGC 2388	17.31 ± 6.08	23.35 ± 4.79
NGC 4041	1.82 ± 0.64	2.62 ± 0.53
NGC 4189	0.25 ± 0.09	0.42 ± 0.09
NGC 4278	0.014 ± 0.005	0.03 ± 0.01
NGC 4293	0.46 ± 0.16	0.64 ± 0.13
NGC 4299	0.18 ± 0.06	0.52 ± 0.11
NGC 4490	0.26 ± 0.09	0.42 ± 0.08
NGC 4651	0.47 ± 0.17	0.87 ± 0.18
NGC 5713	6.04 ± 2.12	8.73 ± 1.78
NGC 6240	101.85 ± 35.78	127.15 ± 25.94
NGC 7217	0.30 ± 0.11	0.49 ± 0.10
NGC 7552	10.99 ± 3.86	15.26 ± 3.11
NGC 7714	8.85 ± 3.11	13.34 ± 2.72
NGC 7771	14.06 ± 4.94	19.47 ± 3.97

person is smaller for the SFR when estimated from both the FUV and $24\mu\text{m}$ luminosity (0.27) rather than from the $24\mu\text{m}$ data (0.30 dex), we believe this as a confirmation of the link between the [CII] emission and star formation activity in a galaxy, that has been reported in this work.

From Eq. 6 we derive the SFR calibration:

$$\text{SFR} = \frac{(L_{\text{[CII]}})^{0.983}}{1.028 \times 10^{40}} \quad (7)$$

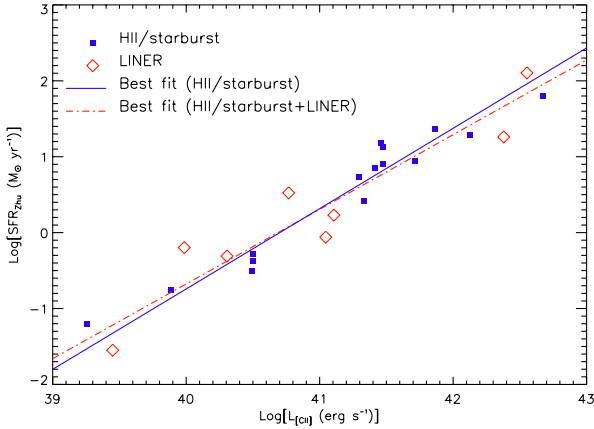
where the SFR and $L_{\text{[CII]}}$ are in units of $M_{\odot} \text{ yr}^{-1}$ and erg s^{-1} , respectively. The SFR calibration factors are derived assuming a [Kroupa \(2001\)](#) IMF. This relation is valid for star-forming, late-type galaxies with a star formation activity in the range $0.03 - 127 M_{\odot} \text{ yr}^{-1}$ and objects with a [CII] luminosity between $39.3 \leq \log L_{\text{[CII]}} [\text{erg s}^{-1}] \leq 42.7$ and a TIR luminosity between $42.1 \leq \log L_{\text{TIR}} [\text{erg s}^{-1}] \leq 45.4$.

Since the residual plot of this SFR relation (see Figure 4, bottom) indicates that the LINER galaxies in our sample contribute most to the observed scatter, we investigate whether a possible AGN contribution to the LINER galaxies introduce a bias to the derived SFR relation. If we calibrate the SFR relation for the 16 HII and starburst galaxies in our sample, we should see a significant difference if the LINER sample indeed introduces a bias, possibly due to a small AGN contribution to the $24\mu\text{m}$ luminosities. From Figure 6 we can deduce that the best fitting line in our sample does not change substantially if we neglect the LINER galaxies for the SFR calibration. This already shows that the LINER sample does not introduce any bias due to a small AGN contribution. Moreover, half of the LINER galaxies are situated below the best fitting line.

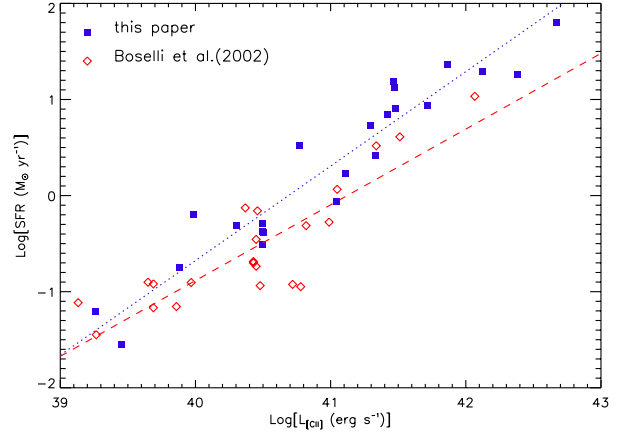
From this tight correlation between the star formation rate and

Table 4. Coefficients and uncertainties of the best fitting line for the relation between $L_{[\text{CII}]}$ and two SFR relations.

Variable	Slope	Intercept	1σ dispersion (dex)
$\text{SFR}_{24\mu\text{m}, \text{Rieke2009}}$	1.040 ± 0.035	-42.535 ± 1.441	0.30
$\text{SFR}_{FUV+24\mu\text{m}, \text{Zhu2008+Kennicutt2009}}$	0.983 ± 0.021	-40.012 ± 0.858	0.27

**Figure 6.** $\text{SFR}_{FUV+24\mu\text{m}}$ (attenuation correction and SFR relation from Zhu et al. 2008 and Kennicutt et al. 2009, respectively) as a function of $L_{[\text{CII}]}$. In this plot, HII/starburst and LINER galaxies are indicated as blue filled squares and red diamonds, respectively. The best fitting line for the HII/starburst sample and the combined HII/starburst+LINER sample are shown as blue plain and red dashed-dotted lines, respectively.

the $[\text{CII}]$ luminosity, we conclude that the $[\text{CII}]$ luminosity is a good star formation rate indicator. The applicability of $[\text{CII}]$ as a star formation rate diagnostic had already been hinted by several authors (Stacey et al. 1991; Pierini et al. 1999; Leech et al. 1999; Boselli et al. 2002; Stacey et al. 2010), but we were able to quantify this correlation in an accurate way. Figure 7 compares our SFR relation to the calibration obtained in Boselli et al. (2002). Since Boselli et al. (2002) assumed a Salpeter (1955) IMF ($\alpha = -2.35$) in the mass range between 0.1 and 100 M_{\odot} , we have divided their calibration coefficient by 1.51, to convert it to the Kroupa (2001) IMF (see Calzetti et al. (2010) for the derivation of the factor 1.51 difference between the Salpeter (1955) and Kroupa (2001) IMF calibrations). For low $[\text{CII}]$ luminosity objects both calibrations are still quite consistent, but for galaxies with an increasing $[\text{CII}]$ luminosity the SFR estimate provided by Boselli et al. (2002) quickly diverges from our estimates up to a factor of ~ 5 for the highest luminosity objects in our sample. This deviation towards higher $[\text{CII}]$ luminosities is probably due to an underestimation of the $H\alpha$ extinction in more luminous galaxies, since the attenuation relations at that time were calibrated without taking into account heavily obscured star formation and thus underestimating the true $H\alpha$ emission. The scatter around the mean trend in our SFR relation is smaller than a factor of 2, while the dispersion in the $[\text{CII}]-H\alpha$ luminosity relation already reaches a factor of ~ 4 . The final uncertainty on the SFR calibration in Boselli et al. (2002) is estimated to be as high as a factor of ~ 10 . We believe the poorly known characteristics of the $[\text{NII}]$ contamination and the attenuation correction at the time

**Figure 7.** The star formation rate as estimated from relation 8 in this paper (blue filled squares) and from the SFR calibration in Boselli et al. (2002). Since Boselli et al. (2002) assumed a Salpeter (1955) IMF ($\alpha = 2.35$) in the mass range between 0.1 and 100 M_{\odot} , we have divided their calibration coefficient by 1.51, to convert it to the Kroupa (2001) IMF we applied. The best fitting lines for our calibration and the one in Boselli et al. (2002) are indicated as blue dotted and red dashed lines, respectively.

Boselli et al. (2002) performed their SFR calibration explain a significant amount of their reported scatter. Benefiting from the increased database of $[\text{CII}]$ observations and exploring other reliable SFR tracers in this paper, we can revise the analysis in Boselli et al. (2002) and conclude that the $[\text{CII}]$ emission is a reliable SFR indicator in most normal star-forming galaxies.

4.2 Applicability

The extension of this SFR relation to ULIRGS should be treated with caution, since a decrease of the $L_{[\text{CII}]}-to-L_{\text{FIR}}$ ratio with increasing warm infrared color for all galaxy types has been observed in many samples (Crawford et al. 1985; Stacey et al. 1991; Malhotra et al. 1997, 2001; Luhman et al. 2003; Verma et al. 2005; Brauher et al. 2008). More specifically, Luhman et al. (2003) report a $[\text{CII}]$ line deficit in a sample of 15 ULIRGS, after they had noticed this trend in a few individual ultra-luminous objects (Luhman et al. 1998). Figure 8 hints at a similar, but weaker, trend for the galaxies in our sample. This effect is probably due to a decrease in efficiency of the photoelectric heating of the gas in strong radiation fields (Malhotra et al. 2001). Other possible explanations for this trend were given in Negishi et al. (2001) and Bergvall et al. (2000). Negishi et al. (2001) suggest an increased collisional de-excitation of $[\text{CII}]$ due to an enhanced gas density, or a decrease in the ionized component for increasing star formation activity. While Bergvall et al. (2000) invokes the self-absorption of $[\text{CII}]$ for galaxies with increasing

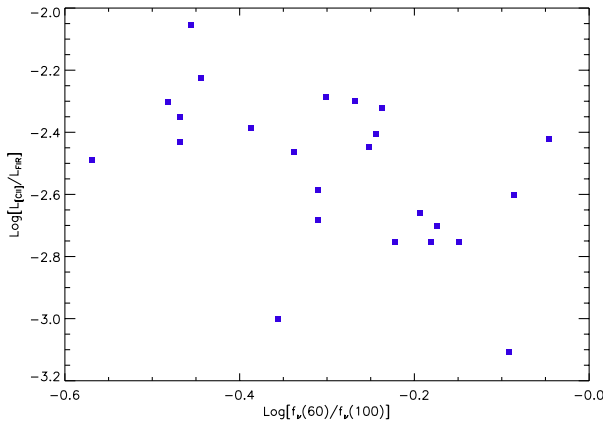


Figure 8. The ratio $L_{\text{[CII]}}$ -to- L_{FIR} as a function of the effective dust temperature, as embodied by the $f_{\nu}(60\mu\text{m})$ -to- $f_{\nu}(100\mu\text{m})$ ratio, where the FIR luminosity was derived following [Helou et al. \(1985\)](#). We notice a decrease of the $L_{\text{[CII]}}$ -to- L_{FIR} ratio with increasing warm dust temperature.

metallicity. Recently, [Papadopoulos et al. \(2010\)](#) and [Rangwala et al. \(2010\)](#) claimed that a high dust optical depth could be the cause of this [CII] line deficit in several galaxies. If this trend in the [CII] line deficit holds for more IR-luminous galaxies, this might have its implications for the reliability of [CII] as a star formation indicator in those objects. Even more recently, [Graciá-Carpio et al. \(2011\)](#) inferred from their Herschel observations a similar line deficit for several other FIR fine structure lines ([NII], [OI], [NIII], [OIII]). They allocate this deficit to a transition between two modes of star formation (in normal disk galaxies and major merger systems) with a different star formation efficiency.

On the other hand, [Pierini et al. \(1999\)](#) also report a decrease in the $L_{\text{[CII]}}$ -to- L_{FIR} ratio for decreasing $H\alpha$ EW. This trend has been observed for more quiescent galaxies with $H\alpha$ EW ≤ 10 Å and can be explained by an increasing contribution from older, less massive stars that heat dust grains and therefore contribute to the FIR-luminosity. The radiation from these stars is not hard enough to substantially heat the dust grains through the photoelectric effect ([Pierini et al. 2003](#)). Since collisions with these photoelectrons are the main heating source for the interstellar gas, this inefficient gas heating will render those galaxies [CII] quiet for an increasing contribution from a more evolved stellar population. This effect makes the extension from the SFR relation to quiescent galaxies not straightforward either. For objects with an extremely low star formation activity, [Pierini et al. \(1999\)](#) also found that the main contribution to the [CII] emission arises from the diffuse neutral interstellar medium. In our current sample, two galaxies (NGC 4293 and NGC 7217) satisfy the criterion $H\alpha$ EW ≤ 10 Å, characterizing a quiescent galaxy ([Kennicutt & Kent 1983](#); [Kennicutt et al. 2008](#)). Since those galaxies do not deviate from the mean trend in the SFR- $L_{\text{[CII]}}$ plot, a larger sample of quiescent galaxies is necessary to further investigate whether our SFR relation is expandable to objects with a lower SFR compared to the galaxies in the present sample.

Because of systematic variations in the $L_{\text{[CII]}}$ -to- L_{FIR} ratio and varying contribution with luminosity from several components (PDRs, diffuse cold neutral and warm ionized gas, HII regions) to the [CII] emission, we should be careful in extending the SFR relation in this paper to more extreme luminosities, on both ends of the luminosity scale. Although the derived star formation relation might not be valid for more extreme cases of star formation activ-

ity (either very quiescent or actively star-forming), this calibration might be useful as an alternative indicator of the star formation rate in objects which lack either UV or IR observations. Since [CII] emission is hardly not affected by attenuation in most cases (currently, Arp 220 is the only object where prominent obscuration effects have been claimed), it might provide an immediate probe of the complete star formation activity.

At high redshift, the behaviour of the $L_{\text{[CII]}}$ -to- L_{FIR} ratio is even different. Ultra luminous objects (ULIRGs; $L_{\text{TIR}} > 10^{12} L_{\odot}$) do not seem to be affected by a [CII] deficit. On the contrary, [Maiolino et al. \(2009\)](#) suggest an enhancement by at least one order of magnitude of the [CII] emission in galaxies at high-redshift compared to local galaxies of the same infrared luminosity. [Maiolino et al. \(2009\)](#) argues that this enhanced [CII] emission could be due to lower metallicities of the ISM in those high-redshift galaxies, which tend to have a lower dust content and therefore a larger [CII] emitting region. Independent of the physical origin of this effect, if confirmed by future observations, the strong [CII] emission from IR luminous high-redshift objects would have great implications for future observations at high redshift. This suggested increase in detectability of the [CII] line at high redshift would also imply an extensive applicability of a SFR relation based on [CII] luminosities, which we will derive in this paper.

Recently, [Stacey et al. \(2010\)](#) reported the detection of the [CII] line in 12 galaxies at redshifts ranging from 1 to 2. They concluded that for starburst-powered galaxies the [CII] emission is comparable to values found in local star-forming galaxies with similar FIR luminosities ($[\text{CII}]/\text{FIR} \sim 3 \times 10^{-3}$), while AGN-dominated galaxies are characterized by [CII]-to-FIR luminosity ratios similar to local ULIRGs ($[\text{CII}]/\text{FIR} \sim 4 \times 10^{-4}$), suggesting that this effect of enhanced [CII] emission only becomes apparent at even higher redshift ($z > 2$). [Stacey et al. \(2010\)](#) also reported that [CII] is a reliable star formation indicator for their heterogeneous sample of starburst-and/or AGN-dominated galaxies in the redshift interval $z = [1, 2]$. At even higher redshifts ($z > 2$), the lower metallicity might influence the temperature and chemical structure of PDRs and thus, the [CII] emission (e.g. [Lequeux et al. 1994](#); [Wolfire 1995](#); [Röllig et al. 2006](#)). Future observations of ULIRGs with Herschel and ALMA will provide insight in the applicability of [CII] as a star formation indicator at high redshift and the validity of the star formation relation derived in this paper.

4.3 Nature of the [CII] emission in galaxies

Besides the first accurate quantitative calibration of the star formation rate against the [CII] luminosity, the tightness of this correlation gives us insight in the origin of the [CII] emission on a global galaxy-scale. In this section, we introduce two possible explanations for the tightness of the SFR-[CII] relation.

Although PDRs are the main contributor to the [CII] emission in most galaxies, a significant fraction also originates in the cold neutral medium (CNM) (i.e. H I clouds, [Kulkarni & Heiles \(1987\)](#); [Madden et al. \(1993\)](#); [Bennett et al. \(1994\)](#); [Wolfire \(1995\)](#); [Sauty et al. \(1998\)](#); [Pierini et al. \(1999, 2001\)](#); [Contursi et al. \(2002\)](#)), the warm ionized medium (WIM) (i.e. diffuse HII regions, [Madden et al. \(1993\)](#); [Heiles \(1994\)](#); [Malhotra et al. \(1997, 2001\)](#); [Leech et al. \(1999\)](#); [Contursi et al. \(2002\)](#)) and to lesser extend also in HII regions ([Stasińska 1990](#)) (see [Boselli et al. 2002](#) for a quantitative analysis of these different contributions). Since the contribution from compact HII regions to the [CII] emission is negligible with respect to other components on galactic scales (e.g. [Stasińska 1990](#);

Malhotra et al. 2000), it is difficult to believe that the contribution from these star-forming regions alone causes this good correlation.

This brings us to a first possible explanation for the strong correlation between [CII] and the SFR. Considering that PDRs are neutral regions of warm dense gas at the boundaries between HII regions and molecular clouds, we think that most of the [CII] emission from PDRs arises from the immediate surroundings of star-forming regions. This might not be surprising, since FUV photons from young O and B stars escaping from the dense HII regions, impinge on the surface of these neutral PDR regions where they will heat the gas through the photoelectric effect on dust grains. We believe that a more or less constant contribution from PDRs to the [CII] emission and the fact that this [CII] emission from PDRs stems from the outer layers of photon-dominated molecular clumps (i.e. at the boundary of molecular clouds and HII regions) might be a reasonable explanation for the tight correlation between the star formation rate and $L_{\text{[CII]}}$. Also, Malhotra et al. (2001) suggest this tight correlation between PDRs and star-forming regions from their analysis of the FUV flux G_0 and gas density n in PDRs. The high PDR temperature and pressure required to fit their data, imply that most of the line and continuum FIR emission arises from the immediate proximity of expanding HII regions. Moreover, mapping of [CII] in the Milky Way (Bennett et al. 1994) and in spatially resolved nearby galaxies (see Sauvage et al. 2005 for an overview) gives indications for a close association between PDRs and ionized gas in these galaxies.

Alternatively, we consider the likely possibility that this tight correlation is not the reflection of shared photoexcitation processes, taking place at the same position within a galaxy. On the contrary, the [CII] emission might not be directly linked to the star formation, but could instead trace the cold ISM being therefore indirectly related to the star formation through the Schmidt law (Kennicutt 1998). Evidence confirming this indirect link is the association of [CII] emission with modest densities and softer FUV radiation fields (e.g. Pineda et al. 2010).

A similar connection between the [CII] emission in a galaxy and the diffuse ISM is typically present in more quiescent objects (Pierini et al. 1999, 2001, 2003), while in star forming galaxies the [CII] line emission is found to mainly arise from PDR's (Crawford et al. 1985; Stacey et al. 1991; Madden et al. 1993). Mapping of [CII] at high resolution is necessary to ascertain the nature of the tight correlation between the SFR and [CII] emission for the normal star-forming galaxies in our sample.

Future observations of spatially resolved objects in the nearby universe and at high redshift of [CII], CO(1-0) and [NII] lines for a sample of galaxies ranging several orders of magnitude in IR-luminosity, will be able to disentangle the different components contributing to the [CII] emission, since the CO(1-0) intensity correlates well with [CII] (Hollenbach & Tielens 1999) in PDRs and [NII] traces the HII regions and the warm ionized medium (Wright et al. 1991; Bennett et al. 1994). Such analysis will enable us to make a distinction between the different sources that contribute to the [CII] emission and, in particular, examine the tight correlation between the star formation rate and [CII] luminosity. High spatial resolution data will be able to distinguish whether [CII] emission from PDRs is closely related to star-forming regions in galaxies or rather the global [CII] emission in a galaxy traces the gas mass. The latter would imply an indirect link between [CII] and the star formation activity in a galaxy through the Schmidt law.

5 CONCLUSIONS

The aim of this paper was to investigate the reliability of [CII] as a SFR indicator. The analysis was conducted in the following way:

- We assembled a sample of 38 galaxies for which ISO [CII], GALEX FUV and MIPS $24\mu\text{m}$ data are available. This initial sample was subdivided according to their nuclear spectral classification (HII/starburst, LINER, AGN). Due to the contaminating $24\mu\text{m}$ emission in AGN hosts, we were unable to directly relate the $24\mu\text{m}$ emission in those objects to the star formation activity. Therefore, the objects with nuclear spectra resembling those of an AGN, were eliminated from our sample.

- For the remaining 24 galaxies in our sample, the SFR was estimated from either the $24\mu\text{m}$ luminosity or a combination of FUV and $24\mu\text{m}$ data. In the latter case the FUV emission is corrected for internal dust attenuation according to Zhu et al. (2008). The SFR calibration in Kennicutt et al. (2009) provides a SFR estimate for this extinction-corrected FUV luminosity. Comparing the dispersions for these two different SFR relations, we found that the SFR correlates best with the [CII] luminosity, when the star formation activity is traced by a combination of those luminosities.

- From the tight correlation of the SFR with the [CII] luminosity (the dispersion around the mean trend is 0.27 dex), we conclude that the [CII] luminosity is a reliable SFR diagnostic in normal, star-forming galaxies in the local universe and find the following SFR calibration:

$$\text{SFR}[\text{M}_{\odot}\text{yr}^{-1}] = \frac{(L_{\text{[CII]}}[\text{erg s}^{-1}])^{0.983}}{1.028 \times 10^{40}} \quad (8)$$

- The extension of this relation to more quiescent galaxies ($H\alpha$ EW ≤ 10 Å) and ultra luminous galaxies (ULIRGs) should be treated with caution, due to a deviation from the $L_{\text{[CII]}}$ -to- L_{FIR} correlation at those extreme ends of the luminosity scale.

- For galaxies in the redshift range $z=[1,2]$, the comparable [CII] luminosities and the enhanced [CII] emission, at even higher redshift, compared to local galaxies with similar FIR luminosities, will render an immense applicability of this SFR relation in future high redshift surveys (both with Herschel and ALMA).

- We believe this tight correlation between the [CII] luminosity and the star formation activity may imply a direct link in photo-excitation processes: the [CII] emission from PDRs arises from the immediate surroundings of star-forming regions (i.e. from the outer layers of photon-dominated clumps) and contributes a more or less constant fraction on a global galaxy-scale. Alternatively, the [CII] emission might equally well trace the star formation in a galaxy, when assuming that the [CII] emission is associated to the cold ISM in a galaxy and, therefore, is indirectly linked to the SFR through the Schmidt law $\Sigma_{\text{SFR}} = \Sigma_{\text{gas}}^{1.4}$.

ACKNOWLEDGEMENTS

We thank the referee for his/her comments, which helped us to improve the paper considerably.

GALEX is a NASA Small Explorer, launched in 2003 April. We gratefully acknowledge NASA's support for construction, operation and science analysis for the GALEX mission, developed in cooperation with the Centre National d'Etudes Spatiales (CNES) of France and the Korean Ministry of Science and Technology.

This work is based in part on observations made with the Spitzer Space Telescope, which is operated by the Jet Propulsion Laboratory, California Institute of Technology under a contract with NASA.

REFERENCES

- Alonso-Herrero, A., Rieke, G. H., Rieke, M. J., Colina, L., Pérez-González, P. G., & Ryder, S. D. 2006, *ApJ*, 650, 835
- Baan, W. A., & Klöckner, H.-R. 2006, *A&A*, 449, 559
- Bakes, E. L. O., & Tielens, A. G. G. M. 1998, *ApJ*, 499, 258
- Bavouzet, N., Dole, H., Le Floch, E., Caputi, K. I., Lagache, G., & Kochanek, C. S. 2008, *A&A*, 479, 83
- Bennett, C. L., et al. 1994, *ApJ*, 434, 587
- Bergvall, N., Masegosa, J., Östlin, G., & Cernicharo, J. 2000, *A&A*, 359, 41
- Bertin, E., & Arnouts, S. 1996, *A&AS*, 117, 393
- Boquien, M., et al. 2010, *ApJ*, 713, 626
- Boselli, A., Gavazzi, G., Lequeux, J., & Pierini, D. 2002, *A&A*, 385, 454
- Boselli, A., Lequeux, J., & Gavazzi, G. 2004, *A&A*, 428, 409
- Boselli, A., Boissier, S., Cortese, L., Buat, V., Hughes, T. M., & Gavazzi, G. 2009, *ApJ*, 706, 1527
- Brauer, J. R., Dale, D. A., & Helou, G. 2008, *ApJS*, 178, 280
- Calzetti, D., et al. 2005, *ApJ*, 633, 871
- Calzetti, D., et al. 2007, *ApJ*, 666, 870
- Calzetti, D., et al. 2010, *ApJ*, 714, 1256
- Cardelli, J. A., Clayton, G. C., & Mathis, J. S. 1989, *ApJ*, 345, 245
- Chabrier, G. 2003, *PASP*, 115, 763
- Clements, E. D. 1983, *MNRAS*, 204, 811
- Contursi, A., et al. 2002, *AJ*, 124, 751
- Crawford, M. K., Genzel, R., Townes, C. H., & Watson, D. M. 1985, *ApJ*, 291, 755
- Crocker, D. A., Baugus, P. D., & Buta, R. 1996, *ApJS*, 105, 353
- Dale, D. A., & Helou, G. 2002, *ApJ*, 576, 159
- Decarli, R., Gavazzi, G., Arosio, I., Cortese, L., Boselli, A., Bonfanti, C., & Colpi, M. 2007, *MNRAS*, 381, 136
- de Vaucouleurs, G., de Vaucouleurs, A., Corwin, H. G., Jr., Buta, R. J., Paturel, G., & Fouqué, P. 1991, *Third Reference Catalogue of Bright Galaxies. Volume I: Explanations and references. Volume II: Data for galaxies between 0^h and 12^h. Volume III: Data for galaxies between 12^h and 24^h.*, by de Vaucouleurs, G.; de Vaucouleurs, A.; Corwin, H. G., Jr.; Buta, R. J.; Paturel, G.; Fouqué, P. Springer, New York, NY (USA), 1991, 2091 p., ISBN 0-387-97552-7, Price US\$ 198.00. ISBN 3-540-97552-7, Price DM 448.00. ISBN 0-387-97549-7 (Vol. I), ISBN 0-387-97550-0 (Vol. II), ISBN 0-387-97551-9 (Vol. III).
- Devost, D., Roy, J.-R., & Drissen, L. 1997, *ApJ*, 482, 765
- Engelbracht, C. W., et al. 2007, *PASP*, 119, 994
- Gao, Y., Wang, Q. D., Appleton, P. N., & Lucas, R. A. 2003, *ApJL*, 596, L171
- Genzel, R., & Cesarsky, C. J. 2000, *ARA&A*, 38, 761
- Gordon, K. D., et al. 2005, *PASP*, 117, 503
- Graciá-Carpio, J., et al. 2011, *APJL*, 728, L7
- Gry, C., et al. 2003, *The ISO Handbook, Volume III - LWS - The Long Wavelength Spectrometer Version 2.1* (June, 2003)
- Hailey-Dunsheath, S., Nikola, T., Stacey, G. J., Oberst, T. E., Parshley, S. C., Benford, D. J., Staguhn, J. G., & Tucker, C. E. 2010, *ApJL*, 714, L162
- Heiles, C. 1994, *ApJ*, 436, 720
- Helou, G., Soifer, B. T., & Rowan-Robinson, M. 1985, *ApJL*, 298, L7
- Helou, G. 2000, *Infrared Space Astronomy, Today and Tomorrow*, 337
- Ho, L. C., Filippenko, A. V., & Sargent, W. L. W. 1997, *ApJS*, 112, 315
- Hodge, P. W., & Kennicutt, R. C., Jr. 1983, *AJ*, 88, 296
- Hollenbach, D. J., Takahashi, T., & Tielens, A. G. G. M. 1991, *ApJ*, 377, 192
- Hollenbach, D. J., & Tielens, A. G. G. M. 1999, *Reviews of Modern Physics*, 71, 173
- Iono, D., et al. 2006, *ApJL*, 645, L97
- Israel, F. P. 1988, *A&A*, 194, 24
- Ivison, R. J., et al. 2010, *A&A*, 518, L35
- Kaufman, M. J., Wolfire, M. G., Hollenbach, D. J., & Luhman, M. L. 1999, *ApJ*, 527, 795
- Kennicutt, R. C., Jr., & Kent, S. M. 1983, *AJ*, 88, 1094
- Kennicutt, R. C., Jr. 1998, *ApJ*, 498, 541
- Kennicutt, R. C., Jr., Lee, J. C., Funes, S. J., José G., Sakai, S., & Akiyama, S. 2008, *ApJS*, 178, 247
- Kennicutt, R. C., et al. 2009, *ApJ*, 703, 1672
- Kroupa, P. 2001, *MNRAS*, 322, 231
- Kroupa, P., & Weidner, C. 2003, *ApJ*, 598, 1076
- Kulkarni, S. R., & Heiles, C. 1987, *Interstellar Processes*, 134, 87
- Leech, K. J., et al. 1999, *MNRAS*, 310, 317
- Lequeux, J., Le Bourlot, J., Pineau des Forets, G., Roueff, E., Boulanger, F., & Rubio, M. 1994, *A&A*, 292, 371
- Leroy, A. K., Walter, F., Brinks, E., Bigiel, F., de Blok, W. J. G., Madore, B., & Thornley, M. D. 2008, *AJ*, 136, 2782
- Luhman, M. L., et al. 1998, *ApJL*, 504, L11
- Luhman, M. L., Satyapal, S., Fischer, J., Wolfire, M. G., Sturm, E., Dudley, C. C., Lutz, D., & Genzel, R. 2003, *ApJS*, 594, 758
- Madden, S. C., Geis, N., Genzel, R., Herrmann, F., Jackson, J., Poglitsch, A., Stacey, G. J., & Townes, C. H. 1993, *ApJ*, 407, 579
- Madden, S. C. 2000, *New Astronomy Review*, 44, 249
- Maiolino, R., et al. 2005, *A&A*, 440, L51
- Maiolino, R., Caselli, P., Nagao, T., Walmsley, M., De Breuck, C., & Meneghetti, M. 2009, *A&A*, 500, L1
- Malhotra, S., et al. 1997, *ApJL*, 491, L27
- Malhotra, S., et al. 2000, *ApJ*, 543, 634
- Malhotra, S., et al. 2001, *ApJ*, 561, 766
- Morrissey, P., et al. 2007, *ApJS*, 173, 682
- Nagamine, K., Wolfe, A. M., & Hernquist, L. 2006, *ApJ*, 647, 60
- Nakagawa, T., Yui, Y. Y., Doi, Y., Okuda, H., Shibai, H., Mochizuki, K., Nishimura, T., & Low, F. J. 1998, *ApJS*, 115, 259
- Negishi, T., Onaka, T., Chan, K.-W., & Roellig, T. L. 2001, *A&A*, 375, 566
- Papadopoulos, P. P., Isaak, K., & van der Werf, P. 2010, *ApJ*, 711, 757
- Pérez-González, P. G., et al. 2006, *ApJ*, 648, 987
- Pierini, D., Leech, K. J., Tuffs, R. J., & Volk, H. J. 1999, *MNRAS*, 303, L29
- Pierini, D., Lequeux, J., Boselli, A., Leech, K. J., & Volk, H. J. 2001, *A&A*, 373, 827
- Pierini, D., Leech, K. J., Volk, H. J. 2003, *A&A*, 397, 871
- Pilbratt, G. L., et al. 2010, *A&A*, 518, L1
- Pineda, J. L., Velusamy, T., Langer, W. D., Goldsmith, P. F., Li, D., & Yorke, H. W. 2010, *A&A*, 521, L19
- Rangwala, N. et al. 2010, in prep.
- Relaño, M., Lisenfeld, U., Pérez-González, P. G., Vílchez, J. M., & Battaner, E. 2007, *ApJL*, 667, L141
- Rieke, G. H., et al. 2004, *ApJS*, 154, 25
- Rieke, G. H., Alonso-Herrero, A., Weiner, B. J., Pérez-González, P. G., Blaylock, M., Donley, J. L., & Marcillac, D. 2009, *ApJ*, 692, 556

- Risaliti, G. 2004, *Memorie della Societa Astronomica Italiana Supplement*, 5, 217
- Röllig, M., Ossenkopf, V., Jeyakumar, S., Stutzki, J., & Sternberg, A. 2006, *A&A*, 451, 917
- Salim, S., et al. 2009, *ApJ*, 700, 161
- Salpeter, E. E. 1955, *ApJ*, 121, 161
- Sauty, S., Gerin, M., & Casoli, F. 1998, *A&A*, 339, 19
- Sauvage, M., Tuffs, R. J., & Popescu, C. C. 2005, *SSR*, 119, 313
- Schlegel, D. J., Finkbeiner, D. P., & Davis, M. 1998, *ApJ*, 500, 525
- Spitzer Observers Manual Version 7.1, SSC, Pasadena
- Stacey, G. J., Geis, N., Genzel, R., Lugten, J. B., Poglitsch, A., Sternberg, A., & Townes, C. H. 1991, *ApJ*, 373, 423
- Stacey, G. J., Hailey-Dunsheath, S., Ferkinhoff, C., Nikola, T., Parshley, S. C., Benford, D. J., Staguhn, J. G., & Fiolet, N. 2010, *ApJ*, 724, 957
- Stark, A. A. 1997, *ApJ*, 481, 587
- Stasińska, G. 1990, *A&AS*, 83, 501
- Tielens, A. G. G. M., & Hollenbach, D. 1985, *ApJ*, 291, 722
- Tully, R. B. 1988, *Nearby Galaxies Catalog*, Cambridge University Press
- Veilleux, S., Kim, D.-C., Sanders, D. B., Mazzarella, J. M., & Soifer, B. T. 1995, *ApJS*, 98, 171
- Verma, A., Charmandaris, V., Klaas, U., Lutz, D., & Haas, M. 2005, *Space Science Reviews*, 119, 355
- Veron-Cetty, M.-P., & Veron, P. 1986, *ApJS*, 66, 335
- Véron-Cetty, M.-P., & Véron, P. 2010, *AAP*, 518, A10
- Wagg, J., Carilli, C. L., Wilner, D. J., Cox, P., De Breuck, C., Menten, K., Riechers, D. A., & Walter, F. 2010, *A&A*, 519, L1
- Werner, M. W., et al. 2004, *ApJS*, 154, 1
- Wolfire, M. G., Hollenbach, D., & Tielens, A. G. G. M. 1989, *ApJ*, 344, 770
- Wolfire, M. G., Hollenbach, D., McKee, C. F., Tielens, A. G. G. M., & Bakes, E. L. O. 1995, *ApJ*, 443, 152
- Wright, E. L., et al. 1991, *ApJ*, 381, 200
- Wu, H., Cao, C., Hao, C.-N., Liu, F.-S., Wang, J.-L., Xia, X.-Y., Deng, Z.-G., & Young, C. K.-S. 2005, *ApJL*, 632, L79
- Zhu, Y.-N., Wu, H., Cao, C., & Li, H.-N. 2008, *ApJ*, 686, 155

This paper has been typeset from a $\text{\TeX}/\text{\LaTeX}$ file prepared by the author.